














Optical conductivity and vibrational spectra of the narrow-gap semiconductor FeGa₃C. Martin ¹, V. A. Martinez,² M. Opačić ³, S. Djurdjić-Mijin ³, P. Mitrić ³, A. Umičević ⁴, A. Poudel ¹, I. Sydoryk ¹, Weijun Ren ^{5,6}, R. M. Martin ⁷, D. B. Tanner ², N. Lazarević ³, C. Petrovic ⁵ and D. Tanasković ³¹*School of Theoretical and Applied Sciences, Ramapo College of New Jersey, Mahwah, New Jersey 07430, USA*²*Department of Physics, University of Florida, Gainesville, Florida 32611, USA*³*Institute of Physics Belgrade, University of Belgrade, Pregrevica 118, 11080 Belgrade, Serbia*⁴*Vinča Institute of Nuclear Sciences, National Institute of the Republic of Serbia, University of Belgrade, P.O. Box 522, 11001 Belgrade, Serbia*⁵*Condensed Matter Physics and Materials Science Department, Brookhaven National Laboratory, Upton, New York 11973, USA*⁶*Shenyang National Laboratory for Materials Science, Institute of Metal Research, Chinese Academy of Sciences, Shenyang 110016, China*⁷*Department of Physics and Astronomy, Montclair State University, Montclair, New Jersey 07043, USA*

(Received 24 February 2023; accepted 10 April 2023; published 26 April 2023; corrected 5 May 2023)

Intermetallic narrow-gap semiconductors have been intensively explored due to their large thermoelectric power at low temperatures and a possible role of strong electronic correlations in their unusual thermodynamic and transport properties. Here we study the optical spectra and vibrational properties of FeGa₃ single crystal. The optical conductivity indicates that FeGa₃ has a direct band gap of ≈ 0.7 eV, consistent with density functional theory (DFT) calculations. Most importantly, we find a substantial spectral weight also below 0.4 eV, which is the energy of the indirect (charge) gap found in resistivity measurements and *ab initio* calculations. We find that the spectral weight below the gap decreases with increasing temperature, which indicates that it originates from the impurity states and not from the electronic correlations. Interestingly, we did not find any signatures of the impurity states in vibrational spectra. The infrared and Raman vibrational lines are narrow and weakly temperature dependent. The vibrational frequencies are in excellent agreement with our DFT calculations, implying a modest role of electronic correlations. Narrow Mössbauer spectral lines also indicate high crystallinity of the sample.

DOI: [10.1103/PhysRevB.107.165151](https://doi.org/10.1103/PhysRevB.107.165151)**I. INTRODUCTION**

Correlated narrow-gap semiconductors represent a class of materials known for their large thermopower at low temperatures and other anomalous transport and thermodynamic properties [1]. Three iron compounds among them, FeSi, FeSb₂, and FeGa₃, share some common features, but also show important differences. FeSi and FeSb₂ behave as insulators only at temperatures $T^* \lesssim 100$ K which corresponds to the energy much smaller than the band gap $E_g \approx 50$ meV [2–4]. A buildup of the in-gap spectral weight at temperatures $k_B T^* \ll E_g$, clearly seen in optical [5–8] and photoemission spectroscopy [9], is a signature of strong electronic correlations [10,11]. A crossover from a nonmagnetic insulator to a bad metal is accompanied by a large increase in the spin susceptibility which obtains Curie-Weiss form above room temperature [12,13]. This crossover leaves fingerprints also in the Raman vibrational spectra which become strongly temperature dependent. The width of vibrational peaks increases several times in the bad-metal region as compared to the low-temperature insulating state [14–16]. At temperatures near 10 K there is a large peak in the thermopower $|S|$ [17,18]. The exact role of the electronic correlations, in-gap states, anisotropy, and phonon drag in colossal thermopower found in FeSb₂ remains a subject of various studies and controversy [19–21].

FeGa₃ has a significantly larger band gap, $E_g \approx 0.4$ eV [22,23], than FeSi and FeSb₂ due to the stronger hybridization between 3*d* orbitals of Fe and 4*p* orbitals of Ga. The electronic structure calculations imply modest contribution of electronic correlations. Density functional theory (DFT) [24] and LDA+*U* [23] calculations give almost the same band structure, while dynamical mean field theory (DFT+DMFT) [25] gives only slightly reduced band gap. Nevertheless, the temperature dependence of dc resistivity is nontrivial: it strongly deviates from a simple activated transport at low temperatures, and features four distinct transport regimes which are associated with a presence of the in-gap states [22,23,25]. For $T \lesssim 5$ K ρ_{dc} has a power law temperature dependence consistent with the variable-range hopping transport driven by the localized in-gap states. In the interval $20 \lesssim T \lesssim 45$ K the charge transport is activated, but corresponds to a small gap of ≈ 40 meV between the in-gap states and the conduction band. Then, following a minimum in ρ_{dc} , there is a metalliclike transport up to ≈ 80 K which presumably corresponds to the regime where most of the in-gap electrons are already transferred to the conduction band. For $T > 300$ K the charge transport is activated, consistent with the wide gap $E_g \approx 0.4$ eV. The measurements show weak sample anisotropy and weak temperature dependence of magnetic susceptibility, whereas the DFT+DMFT calculations give small mass renormalization, as well as strong charge and spin

fluctuations [25]. A maximum in the Seebeck coefficient $|S|$ at $T \approx 15$ K is argued to be a consequence of the phonon-drag effect [23]. In this picture the in-gap states supply free charge carriers and the acoustic phonons cause an additional scattering of the electrons opposite to the direction of a temperature gradient, leading to the large thermoelectric power. Interestingly, to our knowledge, there has been so far only one infrared spectroscopy study of FeGa₃ in polycrystalline samples [26], restricted to room temperature and energies larger than 90 meV.

In this paper, we present infrared and Raman spectroscopy study of FeGa₃ single crystal in the temperature range between 4 and 300 K. The reflectance is measured in the energy interval between 30 and 24 000 cm⁻¹. The infrared and Raman active vibrational frequencies are in excellent agreement with our DFT calculations, indicating good crystallinity and a small influence of electronic correlations. Good crystallinity is corroborated also by measured Mössbauer spectra. The most prominent feature of the optical spectra is the existence of the in-gap states below the charge gap of approximately 0.4 eV. We observe a reduction of the in-gap spectral weight as the temperature increases to 300 K and conclude that this spectral weight originates from the impurities. Details of experimental and numerical methods are presented in Sec. II. The results are shown in Secs. III and IV contains our conclusions.

II. METHODS

Single crystals of FeGa₃ were grown as described previously [22]. For infrared measurements a small crystal was polished until a smooth surface of about 3 mm² area was obtained, then mounted on a helium-flow optical cryostat. The temperature dependence of reflectance was measured between 30 and 24 000 cm⁻¹, using a combination of two Fourier-transform infrared spectrometers: a Bruker 113v for far infrared (30–600 cm⁻¹) and a Bruker Vertex 70, with extended spectral range, from midinfrared to visible (100–24 000 cm⁻¹). Reflectance in visible and ultraviolet (12 000–50 000 cm⁻¹) was measured at room temperature only, using a Perkin-Elmer 650 UV/VIS grating spectrometer. As no temperature dependence was observed above about 12 000 cm⁻¹, all temperatures were merged with room temperature data in visible and ultraviolet parts of the spectrum. To capture correctly the width and line shape of lattice vibrations, the far-IR data were taken with a resolution of 0.5 cm⁻¹, while 2 cm⁻¹ or larger values were used at higher frequencies. Both gold and aluminum mirrors were used for reference, and in order to correct for surface roughness the sample was also gold coated, using a commercial Ted Pella Cressington 108 sputtering machine. Because of the polishing involved, the precise orientation of the electric field (polarization) with respect to the crystallographic axes of the samples is not clearly defined, hence we cannot discuss potential anisotropic optical properties.

Raman scattering measurements were performed using a TriVista557 Raman system, equipped with a nitrogen-cooled CCD detector, in backscattering micro-Raman configuration. Grating configuration was 1800/1800/2400 grooves/mm, in order to achieve the best possible resolution. The 514.5-nm

line of an Ar⁺/Kr⁺ gas laser was used as an excitation source and a microscope objective with factor 50 magnification was used for focusing the beam. All measurements were carried out with laser power less than 1.5 mW at the sample, in order to minimize local heating. Room temperature measurements were done in air, whereas for low temperature measurements the sample was placed in a KONTI CryoVac continuous flow cryostat, with a 0.5-mm-thick window. Spectra were corrected for the Bose factor.

The ⁵⁷Fe-Mössbauer spectrum of the FeGa₃ powdered sample was measured at room temperature in high ($\approx \pm 9$ mm/s) and low ($\approx \pm 2$ mm/s) Doppler velocity range. The spectra were collected in standard transmission geometry in constant acceleration mode using a ⁵⁷Co(Rh) source. The Doppler velocity scale was calibrated by using the Mössbauer spectrum of metallic α -Fe. The spectra were fitted by the RECOIL program [27]. The center shift value (CS) is quoted relative to the α -Fe (CS = 0).

First-principles DFT calculations of electronic structure and phonon frequencies were performed using the open-source QUANTUM-ESPRESSO package [28,29]. We employed the ultrasoft Vanderbilt-type pseudopotentials with Perdew-Burke-Ernzerhof exchange and correlation functional. For the Fe atom we considered 3s, 3p, 3d, and 4s as valence electrons (in total 16), while the Ga valence electrons were taken to be the electrons from 3d, 4s, and 4p orbitals (in total 13). Thus, a minimum of 110 bands was needed to perform the calculations since we have four formula units per unit cell, but we nevertheless considered 128 bands, which is a very convenient number for parallelization purposes. The plane wave kinetic energy cutoff was set to 70 Ry, which proved to be sufficient for all our calculations. The ionic relaxation, self-consistent, and normal mode calculations were performed using the Monkhorst-Pack scheme, with the k mesh of $8 \times 8 \times 8$, which corresponds to 75 k points in the irreducible part of the Brillouin zone. On the other hand, the density of states (DOS) calculation requires a much larger number of k points in order to be accurate, and hence we performed the non-self-consistent calculation with a k mesh of $12 \times 12 \times 12$ in order to calculate the DOS. We used density functional perturbation theory (DFPT) [30] in order to calculate the vibrational frequencies.

III. RESULTS

We first present the band structure calculations. These results are known from the literature, but we nevertheless show them for completeness and in order to put into context the analysis of the experimental data that follow. Then we present optical, Raman, and Mössbauer spectra.

A. DFT band structure

The semiconductor FeGa₃ belongs to the $P4_2/mnm$ space group and it has a tetragonal P -type lattice with lattice parameters $a=6.2628(3)$ Å and $c=6.5546(5)$ Å [31]. In the DFT calculations we used the lattice parameters from the experiment and relaxed only the fractional coordinates of the atoms. These coordinates, shown in Table I, are only slightly adjusted from their measured values.

TABLE I. Nonequivalent atomic positions from the DFT calculation.

Atom	$P\bar{4}n2$	x	y	z
Fe	4 <i>f</i>	0.34367	0.34367	0
Ga1	4 <i>c</i>	0	0.5	0
Ga2	8 <i>j</i>	0.15575	0.15575	0.26295

Figure 1 shows the dispersion relations and the density of states, calculated along the k path Z - R - A - Z - Γ - X - M - Γ in the Brillouin zone. Our results are very similar to previous work [23,32], showing that FeGa₃ is an indirect-gap semiconductor with the calculated band gap of 0.44 eV. The bands around the Fermi level are formed from the hybridized Fe 3*d* and Ga 4*p* orbitals.

B. Optical conductivity and infrared vibrational modes

The reflectance $R(\omega)$ measured at several temperatures between 25 and 300 K is shown in Fig. 2(a). Note that the spectra are shown on a logarithmic frequency scale so that we can distinguish both the low- and high-frequency features. The low-frequency reflectance is close to 1 which indicates a possible presence of the in-gap states that we will discuss in detail below. The far-infrared frequency region is shown on a linear scale in the inset. The peaks in $R(\omega)$ correspond to the infrared-active vibrational modes.

A better insight into the excitation spectrum can be obtained from the real part of the optical conductivity $\sigma_1(\omega)$. It corresponds to the imaginary part of the dielectric function, $\sigma_1(\omega) = \omega\epsilon_2(\omega)/4\pi$, describing the absorption of electromagnetic radiation [33,34]. Figure 2(b) shows $\sigma_1(\omega)$ obtained from the Kramers-Kronig transformation of $R(\omega)$. As this transformation involves integration of $R(\omega)$ from zero to infinity, we used extrapolation of our measurements. At high frequency ($\omega \rightarrow \infty$), the data were bridged with calculations of the dielectric function based on the x-ray photoabsorption, following the procedure described in Ref. [35]. For $\omega < 30 \text{ cm}^{-1}$ we set $R(\omega) = R(30 \text{ cm}^{-1})$, but we checked that $\sigma_1(\omega)$ is not sensitive to the precise form of $R(\omega)$ in the

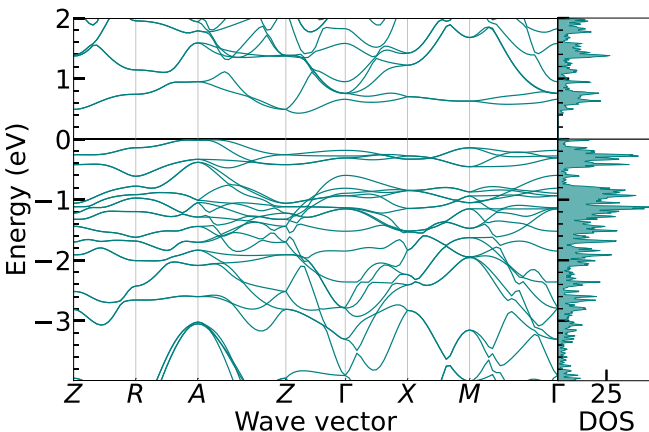


FIG. 1. DFT band structure of FeGa₃ and density of states in units states/(eV f.u.).

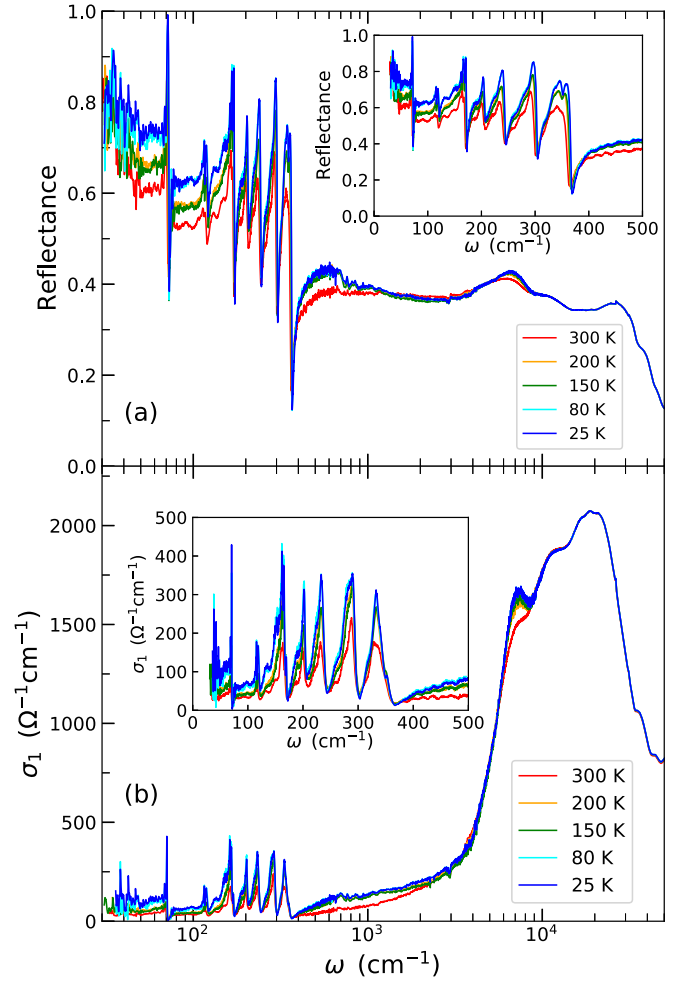


FIG. 2. Reflectance (a) and optical conductivity (b) as a function of frequency in the whole measured frequency range at several temperatures. The insets show the low-frequency data on a linear scale.

limit $\omega \rightarrow 0$. The same result is obtained using the Hagen-Rubens formula, $R(\omega) = 1 - A\sqrt{\omega}$, where A is a constant adjusted to fit the first several points from the measurements [33,34].

The optical conductivity at 25 and 300 K is shown in Fig. 3 on a linear energy (frequency) scale in units of eV. $\sigma_1(\omega)$ rapidly decreases for frequencies $\hbar\omega \lesssim 0.9 \text{ eV}$ (7000 cm^{-1}). This is consistent with the DFT band structure shown in Fig. 1. It gives the smallest direct gap of 0.67 eV near the Z point in the Brillouin zone, but in many regions of the Brillouin zone the gap is between 0.7 and 0.9 eV. At $\hbar\omega = E_g \approx 0.4 \text{ eV}$ the spectral weight is significantly reduced, yet it remains substantial also at $\hbar\omega < E_g$. We note that we did not attempt to calculate the optical spectra since a reliable calculation requires us to include the particle-hole interaction on a level of the Bethe-Salpeter equation, which is a very challenging task even for weakly interacting semiconductors [36,37]. A calculation of the optical spectra of FeGa₃ in the independent-particle approach poorly compares with our experiments [24]. On the other hand, our optical spectra for $\hbar\omega \gtrsim 0.5 \text{ eV}$ are

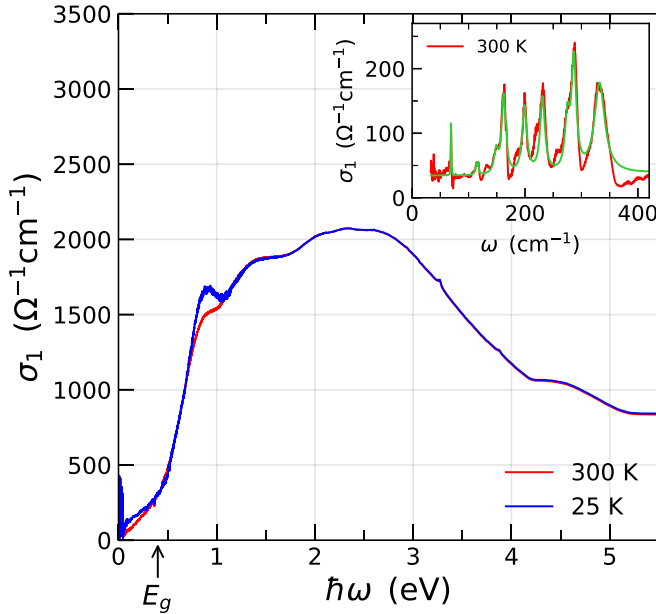


FIG. 3. Optical conductivity as a function of frequency at 25 and 300 K. The inset shows the infrared vibrational modes which are fitted by 11 Lorentzians. The green line corresponds to the cumulative fit.

in rather good agreement with the spectra on polycrystalline samples of Ref. [26].

Evidence that the spectral weight below E_g has origins in the impurity states can be obtained from analysis of the temperature dependence of $\sigma_1(\omega)$. At finite temperatures, in a standard band gap semiconductor a small spectral weight would appear just below E_g due to the phonon assisted excitations. The same amount of the spectral weight would recover just above the band edge, where the absorption becomes slightly lower due to the finite hole (electron) concentration in the valence (conduction) band at finite temperatures [33]. On the other hand, in FeSi and FeSb₂ a spectral gap is closed at higher temperatures due to the strong correlation effects. In this case, transfers of the spectral weight occur over the energy range much larger than the band gap. However, in our case the spectral weight at $T = 300$ K is reduced both below and above E_g [see Figs. 2(b) and 3]. The reduction of the spectral weight below E_g should correspond to the depopulation of the impurity band, which leads to the reduction in the light absorption for subgap energies [25]. Hence, we conclude that the spectral weight below E_g is due to impurity states. We note that a small surplus of Fe atoms in comparison to the stoichiometric ratio is found in wavelength dispersive x-ray spectroscopy [23]. Our conclusion is in line with the statement that the transfer of the electrons from the impurity states to the conduction band is a likely cause of the anomalous $d\rho/dT > 0$ resistivity temperature dependence around 100 K [20,25].

We now turn our attention to the far-infrared part of the spectrum from 50 to 350 cm^{-1} , which contains infrared vibrational modes. From the inset of Fig. 2(b) it appears that most of the phonon peaks are rather broad. However, that is not the case since several peaks, in fact, consist of two vi-

TABLE II. Irreducible representation of infrared-active modes and their frequencies. The measured frequencies are obtained at 300 K. Numerical values are obtained within DFPT calculation.

Irred. rep.	Expt. (cm^{-1})	Calc. (cm^{-1})
$E_u^{1,2}$	69.00	76.08
A_{2u}^1	113.50	107.61
$E_u^{3,4}$	117.50	116.18
$E_u^{5,6}$	149.85	161.78
A_{2u}^2	162.2	162.28
$E_u^{7,8}$	166.99	168.69
$E_u^{9,10}$	199.50	201.71
$E_u^{11,12}$	231.50	229.45
$E_u^{13,14}$	275.00	281.2
A_{2u}^3	287.30	296.61
$E_u^{15,16}$	332.50	329.0

brational modes with very close frequencies. The space group $P4_2/mmm$ has the corresponding point group $D_{4h}(4/mmm)$. Thus, all the normal modes are classified according to irreducible representations of $D_{4h}(4/mmm)$. The factor group analysis predicts 12 Raman and 11 infrared-active modes, along with ten silent and two acoustic modes:

$$\begin{aligned}
 \Gamma_{\text{Raman}} &= 3A_{1g} + 4E_g + 2B_{1g} + 3B_{2g}, \\
 \Gamma_{\text{IR}} &= 3A_{2u} + 8E_u, \\
 \Gamma_{\text{silent}} &= 2A_{2g} + 2A_{2u} + 4B_{1u} + 2B_{2u}, \\
 \Gamma_{\text{acoustic}} &= A_{2u} + E_u.
 \end{aligned} \tag{1}$$

The experimental data at 300 K are fitted with 11 Lorentz profile lines. Their cumulative contribution to the spectra is shown in green color in the inset of Fig. 3. A complete list of the corresponding phonon frequencies is shown in Table II. These frequencies were obtained at 300 K, but we see from the inset in Fig. 2(b) that the temperature dependence of the frequencies is weak. The changes are of the order of 1% in the temperature range between 25 and 300 K. The frequencies calculated within DFPT are in excellent agreement with measured frequencies. This implies that a crystallinity of the sample is very good, even though some surplus of Fe iron atoms is expected in comparison to the ideal composition [23]. In addition, excellent agreement between the calculated and measured frequencies indicates that the electronic correlations beyond the DFT are not strong, in line with the conclusions from DFT+ U [23] and DFT+DMFT [25] calculations.

C. Raman spectra

There are 12 Raman-active modes in FeGa₃ [see Eq. (1)]. Wyckoff positions of the atoms, their contributions to the Γ -point phonons, and the corresponding tensors for Raman active modes are given in Table III. Since observability of the Raman-active modes in backscattering configuration of the experiment strongly depends on the orientation of the sample, we first performed orientation dependent measurements. This was done by rotating the sample in the steps of 10°. The orientation of the sample which provided the best observability

TABLE III. Contributions of each atom to the Γ -point phonons for the $P4_2/mnm$ space group and the corresponding tensors for Raman active modes.

Space group $P4_2/mnm$		
Atoms	Irreducible representations	
Fe (4 <i>f</i>)	$A_{1g} + A_{2g} + A_{2u} + B_{1g}$ $+B_{1u} + B_{2g} + E_g + 2E_u$	
Ga (4 <i>c</i>)	$A_{1u} + A_{2u} + B_{1u} + B_{2u} + 4E_u$	
Ga (8 <i>j</i>)	$2A_{1g} + A_{1u} + A_{2g} + A_{2u} + B_{1g}$ $+2B_{1u} + 2B_{2g} + B_{2u} + 3E_g + 3E_u$	
$A_{1g} = \begin{pmatrix} a & 0 & 0 \\ 0 & a & 0 \\ 0 & 0 & b \end{pmatrix}$	$B_{1g} = \begin{pmatrix} c & 0 & 0 \\ 0 & -c & 0 \\ 0 & 0 & 0 \end{pmatrix}$	$B_{2g} = \begin{pmatrix} 0 & d & 0 \\ d & 0 & 0 \\ 0 & 0 & 0 \end{pmatrix}$
${}^1E_g = \begin{pmatrix} c & 0 & 0 \\ 0 & 0 & e \\ 0 & e & 0 \end{pmatrix}$	${}^2E_g = \begin{pmatrix} 0 & 0 & -e \\ 0 & 0 & 0 \\ -e & 0 & 0 \end{pmatrix}$	

of Raman modes of various symmetries was used in further measurements.

Raman spectra of FeGa₃ single crystals, measured from the (011) plane of the sample, at temperature $T = 100$ K, for polarization plane angles within the range of 0° and 180° are presented in Fig. 4. We have identified 10 out of 12 Raman active modes. The assignment of modes was done in accordance with DFT calculations and polarization measurements. Peaks that exhibit the same polarization dependence were assigned with the same symmetry. Consequently, peaks at 146.58 and 331.80 cm^{-1} were assigned as A_{1g} and peaks at 127.99 and 269.98 cm^{-1} were assigned as B_{1g} . The phonon lines at 138.96, 179.01, and 264.40 cm^{-1} are assigned as E_g , whereas modes at 161.67, 238.27, and 321.43 cm^{-1} correspond to the B_{2g} symmetry modes. The full list of measured phonon

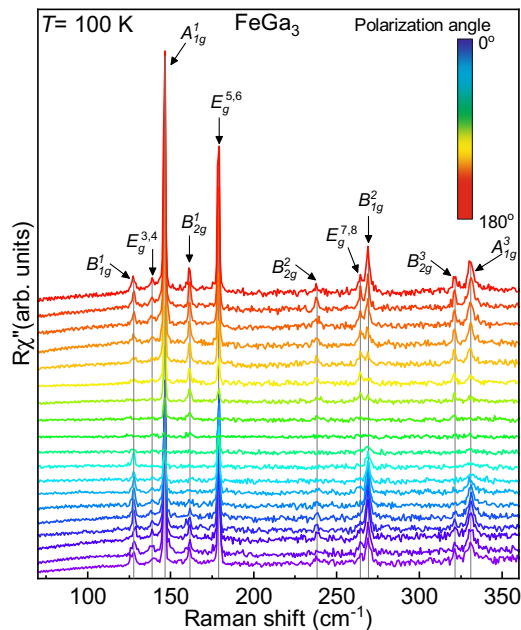


FIG. 4. Polarization-dependent Raman spectra of FeGa₃ single crystals. Measurements were performed with measuring step of 10° at temperature $T = 100$ K.

TABLE IV. Experimental Raman frequencies measured at 100 K and the corresponding values calculated within DFPT.

Irred. rep.	Expt. (cm^{-1})	Calc. (cm^{-1})
$E_g^{1,2}$		86.81
B_{1g}^1	127.99	125.52
$E_g^{3,4}$	138.96	139.06
A_{1g}^1	146.58	145.89
B_{1g}^2	161.67	161.51
$E_g^{5,6}$	179.01	165.09
A_{1g}^2		180.12
B_{2g}^2	238.27	239.62
$E_g^{7,8}$	264.40	258.94
B_{1g}^2	269.28	262.96
B_{2g}^3	321.43	318.53
A_{1g}^3	331.80	322.41

frequencies, along with their calculated values, is shown in Table IV.

There is a very good agreement between experimental and calculated phonon frequencies, with a discrepancy of less than 8%. A close match in experimental and theoretical results is not surprising knowing that the investigated material is semiconducting, with moderate electronic correlations. All of the observed phonon lines are sharp, with the full width at half maximum (FWHM) ≈ 2 cm^{-1} , and weakly temperature dependent. This indicates a good crystallinity of the sample and absence of a metal-insulator transition or magnetic ordering.

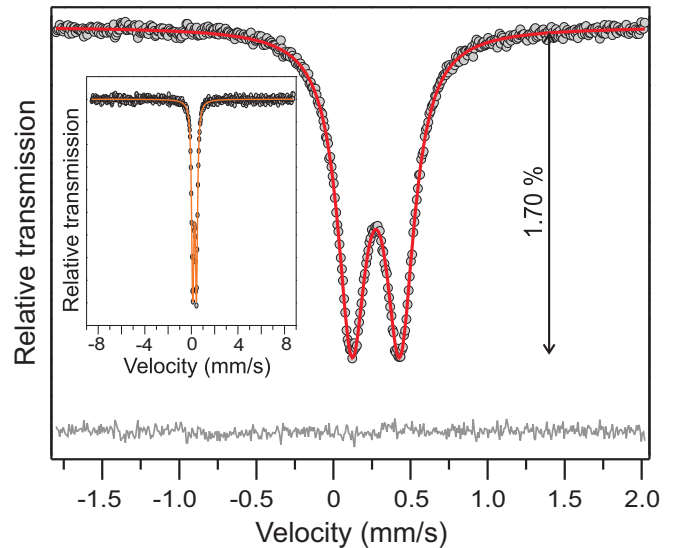


FIG. 5. Room temperature ${}^{57}\text{Fe}$ -Mössbauer spectra of the FeGa₃ sample recorded in the low-velocity range. Experimental data are presented by the solid circles and the fit is given by the red solid line. The difference (Calc. – Expt.) is shown by the dark gray line at the bottom of the figure. The vertical arrow denotes the relative position of the lowest experimental point with respect to the background (relative absorption of 1.70%). The absolute difference is less than 0.05%. The inset shows the room temperature spectrum of the FeGa₃ sample recorded within the high-velocity range. The orange line is just a guide for the eye.

D. Mössbauer spectra

The ^{57}Fe -Mössbauer spectroscopy was used to investigate quality and ordering of the prepared sample and to check for the presence of Fe-based impurity phases. The ^{57}Fe -Mössbauer spectra of the FeGa_3 are presented in Fig. 5. The spectrum recorded in the low-velocity range showed two absorption lines (doublet). In the spectrum recorded in the high-velocity range, beside the observed doublet, there is no indication of the magnetic hyperfine splitting. The thickness corrected FeGa_3 spectrum recorded in the low-velocity range was fitted with one Lorentzian-shaped doublet using the RECOIL program [27]. The obtained Mössbauer parameters for the measured doublet are center shift $\text{CS} = 0.28$ mm/s, quadrupole splitting $\Delta = 0.31$ mm/s, and FWHM of the Lorentzian lines is 0.22 mm/s. The obtained results closely match the hyperfine parameters for FeGa_3 from the literature [38–42]. A very small broadening of the resonance lines observed in the experiment is a strong indication that the sample is very well ordered and of high crystallinity.

IV. CONCLUSIONS

In summary, we have performed optical, Raman, and Mössbauer spectroscopy measurements of a narrow-gap semiconductor FeGa_3 , along with DFT band structure and vibrational frequencies calculation. We find that the optical conductivity decreases for frequencies below $\hbar\omega \approx 0.9$ eV consistent with the direct band gap observed in DFT calculations. Our most important finding is the appearance of the optical spectral weight below the charge (indirect) gap $E_g \approx 0.4$ eV. At room temperature the spectral weight below E_g diminishes as compared to the one at $T = 25$ K. Therefore,

we conclude that this spectral weight originates from the impurities and not from the correlation effects. Interestingly, we do not find signatures of the impurities in the vibrational spectra. Both the infrared and Raman lines are very narrow, as well as the Mössbauer spectral lines, which implies a good crystallinity of the sample. The calculated vibrational frequencies are in a very good agreement with the measurements, which indicates that the electronic correlations in FeGa_3 are not strong, in line with previous studies.

ACKNOWLEDGMENTS

A.U. acknowledges fruitful discussions with V. Ivanovski. C.M. acknowledges funding from the Research Honors Program at Ramapo College of New Jersey. M.O., S.Dj.-M., P.M., N.L., and D.T. acknowledge funding provided by the Institute of Physics Belgrade, through a grant by the Ministry of Science, Technological Development, and Innovation of the Republic of Serbia. A.U. acknowledges support provided by the Vinča Institute of Nuclear Sciences, through an agreement with the Ministry of Science, Technological Development, and Innovation of the Republic of Serbia. C.P. acknowledges support by the U.S. Department of Energy, Basic Energy Sciences, Division of Materials Science and Engineering, under Contract No. DE-SC0012704 (BNL), and W.R. was supported by the National Natural Science Foundation of China under Grants No. 51671192 and No. 51531008 (Shenyang). Numerical simulations were performed on the PARADOX supercomputing facility at the Scientific Computing Laboratory, National Center of Excellence for the Study of Complex Systems, Institute of Physics Belgrade.

-
- [1] J. M. Tomczak, Thermoelectricity in correlated narrow-gap semiconductors, *J. Phys.: Condens. Matter* **30**, 183001 (2018).
 - [2] Z. Schlesinger, Z. Fisk, H.-T. Zhang, M. B. Maple, J. DiTusa, and G. Aeppli, Unconventional Charge Gap Formation in FeSi, *Phys. Rev. Lett.* **71**, 1748 (1993).
 - [3] C.-H. Park, Z.-X. Shen, A. G. Loeser, D. S. Dessau, D. G. Mandrus, A. Migliori, J. Sarrao, and Z. Fisk, Direct observation of a narrow band near the gap edge of FeSi, *Phys. Rev. B* **52**, R16981 (1995).
 - [4] C. Petrovic, J. W. Kim, S. L. Bud'ko, A. I. Goldman, P. C. Canfield, W. Choe, and G. J. Miller, Anisotropy and large magnetoresistance in the narrow-gap semiconductor FeSb₂, *Phys. Rev. B* **67**, 155205 (2003).
 - [5] A. Damascelli, K. Schulte, D. van der Marel, and A. A. Menovsky, Infrared spectroscopic study of phonons coupled to charge excitations in FeSi, *Phys. Rev. B* **55**, R4863 (1997).
 - [6] M. A. Chernikov, L. Degiorgi, E. Felder, S. Paschen, A. D. Bianchi, H. R. Ott, J. L. Sarrao, Z. Fisk, and D. Mandrus, Low-temperature transport, optical, magnetic and thermodynamic properties of Fe_{1-x}Co_xSi, *Phys. Rev. B* **56**, 1366 (1997).
 - [7] A. Perucchi, L. Degiorgi, R. Hu, C. Petrovic, and V. F. Mitrović, Optical investigation of the metal-insulator transition in FeSb₂, *Eur. Phys. J. B* **54**, 175 (2006).
 - [8] A. Herzog, M. Marutzky, J. Sichelschmidt, F. Steglich, S. Kimura, S. Johnsen, and B. B. Iversen, Strong electron correlations in FeSb₂: An optical investigation and comparison with RuSb₂, *Phys. Rev. B* **82**, 245205 (2010).
 - [9] M. Arita, K. Shimada, Y. Takeda, M. Nakatake, H. Namatame, M. Taniguchi, H. Negishi, T. Oguchi, T. Saitoh, A. Fujimori, and T. Kanomata, Angle-resolved photoemission study of the strongly correlated semiconductor FeSi, *Phys. Rev. B* **77**, 205117 (2008).
 - [10] J. M. Tomczak, K. Haule, T. Miyake, A. Georges, and G. Kotliar, Thermopower of correlated semiconductors: Application to FeAs₂ and FeSb₂, *Phys. Rev. B* **82**, 085104 (2010).
 - [11] J. M. Tomczak, K. Haule, and G. Kotliar, Signatures of electronic correlations in iron silicide, *Proc. Natl. Acad. Sci. USA* **109**, 3243 (2012).
 - [12] V. Jaccarino, G. K. Wertheim, J. H. Wernick, L. R. Walker, and S. Aarj, Paramagnetic excited state of FeSi, *Phys. Rev.* **160**, 476 (1967).
 - [13] T. Koyama, Y. Fukui, Y. Muro, T. Nagao, H. Nakamura, and T. Kohara, Nuclear quadrupole resonance study of the electronic properties of the narrow-gap semiconductor FeSb₂, *Phys. Rev. B* **76**, 073203 (2007).
 - [14] A.-M. Racu, D. Menzel, J. Schoenes, and K. Doll, Crystallographic disorder and electron-phonon coupling in Fe_{1-x}Co_xSi single crystals: Raman spectroscopy study, *Phys. Rev. B* **76**, 115103 (2007).

- [15] N. Lazarević, Z. V. Popović, R. Hu, and C. Petrovic, Evidence for electron-phonon interaction in $\text{Fe}_{1-x}\text{M}_x\text{Sb}_2$ ($M = \text{Co}$ and Cr ; $0 \leq x \leq 0.5$) single crystals, *Phys. Rev. B* **81**, 144302 (2010).
- [16] N. Lazarević, M. M. Radonjić, D. Tanasković, R. Hu, C. Petrovic, and Z. V. Popović, Lattice dynamics of FeSb_2 , *J. Phys.: Condens. Matter* **24**, 255402 (2012).
- [17] B. C. Sales, E. C. Jones, B. C. Chakoumakos, J. A. Fernandez-Baca, H. E. Harmon, J. W. Sharp, and E. H. Volckmann, Magnetic, transport, and structural properties of $\text{Fe}_{1-x}\text{Ir}_x\text{Si}$, *Phys. Rev. B* **50**, 8207 (1994).
- [18] P. Sun, N. Oeschler, S. Johnsen, B. B. Iversen, and F. Steglich, Huge thermoelectric power factor: FeSb_2 versus FeAs_2 and RuSb_2 , *Appl. Phys. Express* **2**, 091102 (2009).
- [19] C. C. Homes, Q. Du, C. Petrovic, W. H. Brito, S. Choi, and G. Kotliar, Unusual electronic and vibrational properties in the colossal thermopower material FeSb_2 , *Sci. Rep.* **8**, 11692 (2018).
- [20] M. Battiato, J. M. Tomczak, Z. Zhong, and K. Held, Unified Picture for the Colossal Thermopower Compound FeSb_2 , *Phys. Rev. Lett.* **114**, 236603 (2015).
- [21] Q. Du, L. Wu, H. Cao, C.-J. Kang, C. Nelson, G. L. Pascut, T. Besara, T. Siegrist, K. Haule, G. Kotliar, I. Zaliznyak, Y. Zhu, and C. Petrovic, Vacancy defect control of colossal thermopower in FeSb_2 , *npj Quantum Mater.* **6**, 13 (2021).
- [22] Y. Hadano, S. Narazu, M. A. Avila, T. Onimaru, and T. Takabatake, Thermoelectric and magnetic properties of a narrow-gap semiconductor FeGa_3 , *J. Phys. Soc. Jpn.* **78**, 013702 (2009).
- [23] M. Wagner-Reetz, D. Kasinathan, W. Schnelle, R. Cardoso-Gil, H. Rosner, Y. Grin, and P. Gille, Phonon-drag effect in FeGa_3 , *Phys. Rev. B* **90**, 195206 (2014).
- [24] Z. P. Yin and W. E. Pickett, Evidence for a spin singlet state in the intermetallic semiconductor FeGa_3 , *Phys. Rev. B* **82**, 155202 (2010).
- [25] M. B. Gamža, J. M. Tomczak, C. Brown, A. Puri, G. Kotliar, and M. C. Aronson, Electronic correlations in FeGa_3 and the effect of hole doping on its magnetic properties, *Phys. Rev. B* **89**, 195102 (2014).
- [26] Y. V. Knyazev and Y. I. Kuz'min, The study of the structure of the electronic states of the FeGa_3 and RuGa_3 compounds by optical spectroscopy method, *Phys. Solid State* **59**, 2244 (2017).
- [27] K. Lagarec and D. G. Rancourt, *RECOIL, Mössbauer spectral analysis software for Windows* (University of Ottawa, Ottawa, Canada, 1998).
- [28] P. Giannozzi, S. Baroni, N. Bonini, M. Calandra, R. Car, C. Cavazzoni, D. Ceresoli, G. L. Chiarotti, M. Cococcioni, I. Dabo, A. D. Corso, S. de Gironcoli, S. Fabris, G. Fratesi, R. Gebauer, U. Gerstmann, C. Gougousis, A. Kokalj, M. Lazzeri, L. Martin-Samos *et al.*, Quantum espresso: a modular and open-source software project for quantum simulations of materials, *J. Phys.: Condens. Matter* **21**, 395502 (2009).
- [29] P. Giannozzi, O. Andreussi, T. Brumme, O. Bunau, M. B. Nardelli, M. Calandra, R. Car, C. Cavazzoni, D. Ceresoli, M. Cococcioni, N. Colonna, I. Carnimeo, A. D. Corso, S. de Gironcoli, P. Delugas, R. A. DiStasio, A. Ferretti, A. Floris, G. Fratesi, G. Fugallo *et al.*, Advanced capabilities for materials modelling with quantum espresso, *J. Phys.: Condens. Matter* **29**, 465901 (2017).
- [30] S. Baroni, S. de Gironcoli, A. Dal Corso, and P. Giannozzi, Phonons and related crystal properties from density-functional perturbation theory, *Rev. Mod. Phys.* **73**, 515 (2001).
- [31] U. Häussermann, M. Boström, P. Viklund, O. Rapp, and T. Björnängen, FeGa_3 and RuGa_3 : Semiconducting Intermetallic Compounds, *J. Solid State Chem.* **165**, 94 (2002).
- [32] Y. Imai and A. Watanabe, Electronic structures of semiconducting FeGa_3 , RuGa_3 , OsGa_3 , and RuIn_3 with the CoGa_3 - or the FeGa_3 -type structure, *Intermetallics* **14**, 722 (2006).
- [33] F. Wooten, *Optical Properties of Solids* (Academic Press, New York, 1972).
- [34] D. B. Tanner, *Optical Effects in Solids* (Cambridge University Press, New York, 2019).
- [35] D. B. Tanner, Use of x-ray scattering functions in Kramers-Kronig analysis of reflectance, *Phys. Rev. B* **91**, 035123 (2015).
- [36] S. Albrecht, L. Reining, R. Del Sole, and G. Onida, *Ab Initio* Calculation of Excitonic Effects in the Optical Spectra of Semiconductors, *Phys. Rev. Lett.* **80**, 4510 (1998).
- [37] M. Rohlfing and S. G. Louie, Electron-hole excitations and optical spectra from first principles, *Phys. Rev. B* **62**, 4927 (2000).
- [38] G. L. Whittle, P. E. Clark, and R. Cywinski, Vacancies and site occupation in Co-Ga-Fe alloys (Mössbauer study), *J. Phys. F* **10**, 2093 (1980).
- [39] I. Dézsi, I. Szűcs, C. Fetzter, and W. Keune, The local interactions of Co and Fe in β -phase $\text{Co}_x\text{Ga}_{(1-x)}$, *Acta Mater.* **46**, 3299 (1998).
- [40] N. Tsujii, H. Yamaoka, M. Matsunami, R. Eguchi, Y. Ishida, Y. Senba, H. Ohashi, S. Shin, T. Furubayashi, H. Abe, and H. Kitazawa, Observation of energy gap in FeGa_3 , *J. Phys. Soc. Jpn.* **77**, 024705 (2008).
- [41] G. R. Hearne, S. Bhattacharjee, B. P. Doyle, M. A. M. Ahmed, P. Musyimi, E. Carleschi, and B. Joseph, Pressure-induced disruption of the local environment of Fe-Fe dimers in FeGa_3 accompanied by metallization, *Phys. Rev. B* **98**, 020101(R) (2018).
- [42] D. Mondal, C. Kamal, S. Banik, A. Bhakar, A. Kak, G. Das, R. V. R., A. Chakrabarti, and T. Ganguli, Structural and electronic properties of $\text{Fe}(\text{Al}_x\text{Ga}_{1-x})_3$ system, *J. Appl. Phys.* **120**, 165102 (2016).

Correction: A typographical error in the fourth affiliation was introduced during the production cycle and has been fixed.